Composites Part B 166 (2019) 428–435

Contents lists available at ScienceDirect

Composites Part B

journal homepage: www.elsevier.com/locate/compositesb

Experimental study on thermal expansion coefficient of composite multi-layered flaky gun propellants

Taixin Liang[a,*], Le Qi[a], Zhongliang Ma[a], Zhongliang Xiao[b], Yang Wang[c], Hu Liu[d,e], Jiaoxia Zhang[d,f], Zhanhu Guo[d], Chuntai Liu[e,****], Wei Xie[g,***], Tao Ding[h,**], Na Lu[c,*****]

[a] School of Environment and Safety Engineering. The North University of China, Taiyuan, 030051, China
[b] School of Chemical Engineering. The Nanjing University of Science and Technology, Nanjing, 210094, China
[c] Lyles School of Civil Engineering, School of Materials Engineering, Birck Nanotechnology Center, Purdue University, West Lafayette, IN, 47906, USA
[d] Integrated Composites Laboratory (ICL), Department of Chemical & Biomolecular Engineering, University of Tennessee, Knoxville, TN, 37996, USA
[e] Key Laboratory of Materials Processing and Mold (Zhengzhou University), Ministry of Education; National Engineering Research Center for Advanced Polymer Processing Technology, Zhengzhou University, Zhengzhou, 450002, China
[f] School of Material Science and Engineering, Jiangsu University of Science and Technology, Zhenjiang, Jiangsu, 212003, China
[g] Key Laboratory of Lightweight and Reliability Technology for Engineering Vehicle, The Education Department of Hunan Province, Changsha University of Science & Technology, Changsha, 410114, China
[h] College of Chemistry and Chemical Engineering, Henan University, Kaifeng, 475004, China

ARTICLE INFO

Keywords:
Flaky gun propellant
Variable burning-rate gun propellant
Thermal expansion coefficient
TMA (thermal mechanical analyzer) test

ABSTRACT

Improving the burning progressivity is an effective approach to improve the muzzle velocities of projectile of a gun. Composite multi-layered flaky gun propellant is a combination of a fast-burning inner layer and a slow-burning outer layer. It has an obvious burning progressivity which decreases the pressure in bore and increases the muzzle velocity, thus this characteristic is widely concerned by the research of gun propellant. The thermal expansion coefficient of composite multi-layered gun propellant has a significant influence on the combustion performance. Therefore, understanding the thermal expansion properties of the composite multi-layered gun propellant is important. In this study, the thermal expansion coefficients were measured by thermal mechanical analyzer (TMA) for a three-layered flaky gun propellant, and the influence of laminating and coating flaky gun propellant on thermal expansion coefficient was investigated. The results showed that the slow-burning layers had a higher thermal expansion coefficient than the faster-burning layers, the thermal expansion coefficient of slow-burning layers was 4–5 times bigger than that of fast-burning layers, and the order of magnitudes was $1 \times 10^{-5} K^{-1}$. The laminating and coating had a great influence on the thermal expansion coefficient of flaky gun propellant, the thermal expansion coefficient of laminate sample was 10 times greater than that of the original sample, and the order of magnitudes for two layers and three layers propellant reached $1 \times 10^{-4} K^{-1}$. Furthermore, the theoretical relations between the thermal expansion coefficient of axial and the thermal expansion coefficient of the fast and slow burning layer were derived.

1. Introduction

The composite multi-layered flaky gun propellant is a kind of flaky gun propellant which is composed of a fast-burning layer and slow-burning layer. It is a kind of variable burning-rate gun propellant with a "sandwich type" structure. The gun propellant was proved to have a good burning progressivity [1,2]. Because of the differences in the ratio of the fast-burning layers and slow-burning layers, the combustion speeds and some other physical properties (such as the thermal expansion coefficient) are different. When using and storing gun propellants, the environment temperature can be changed. Because of different thermal expansion coefficients in the composite multi-layered

* Corresponding author.
** Corresponding author.
*** Corresponding author.
**** Corresponding author.
***** Corresponding author.
E-mail addresses: liangtx2006@126.com (T. Liang), ctliu@zzu.edu.cn (C. Liu), xwxw00@163.com (W. Xie), dingtao@henu.edu.cn (T. Ding), luna@purdue.edu (N. Lu).

https://doi.org/10.1016/j.compositesb.2019.02.024
Received 6 November 2018; Received in revised form 2 January 2019; Accepted 11 February 2019
Available online 18 February 2019
1359-8368/

flaky gun propellant, the stress state of the interface between fast-burning layer and slow-burning layer changes, and thus affects the mechanical properties and combustion performance. As a result, the thermal expansion coefficient plays a significant role in the research of flaky gun propellant.

As an inherent characteristic of gun propellant, the thermal expansion coefficient of the material remains constant winthin a small temperature range. However, if the temperature varies widely, the value will change. Many optical methods were used to measure the thermal expansion coefficient before year of 2000. For example, The University of California created a simplified mathematical model for the measurement of thermal expansion coefficient of thin sheet materials with a holographic technique. This experimental apparatus can test both above and below room temperature, but it needs use different experimental apparatus structures [3]. Okaji et al. used an absolute interferometric dilatometer to measure the thermal expansion coefficient of copper in the temperature range of 20–300 K, the test results showed that the improved interferometer enabled more accurate length measurement than the previous one [4]. Strycker et al. demonstrated that it was possible to measure homogeneous thermal strain fields on steel samples with digital image correlation technique. But the measured data is a point set, not a curve, which is not convenient for data processing [5]. There is a close relationship between the thermal expansion coefficients and the glass transition temperature for double-based gun propellant, thus studying the glass transition temperature by measuring the thermal expansion coefficients is an important research method [6–9]. Also, negative thermal expansion of materials has attracted considerable attentions [10–12]. Many metallic compound materials have demonstrated negative thermal expansion, such as $Y_2Mo_3O_{12}$ and $NbOPO_4$. These metallic compound materials were measured by X-ray diffraction (XRD) method, the results show that these materials represent negative thermal expansion in some rising temperature ranges on a specific crystal plane [13–15]. Also, the XRD method was applied for the determination of thermal expansion coefficient [16,17], and the density was measured [18]. Since the discovery of graphene, various properties of graphene were tested. One of its significant properties is its negative thermal (0–300 K) expansion and isotropic behavior [19]. The negative thermal expansion is possibly caused by particular molecular structure of materials, such as non-metallic materials with laminar molecular structure [20], composites with needle-like inclusion also exhibit negative thermal expansion at any length scale including microscale [21]. Some researchers analyzed the uniaxial negative thermal expansion in an organic complex, it showed that the sliding of layers may cause the negative thermal expansion [22,23]. Tada et al. used microelectromechanical systems (MENS) to determine the difference in thermal expansion coefficients between poly-Si and SiO_2 thin films in the temperature range of ~293–1123 K and they showed that the thermal expansion coefficient of poly-Si thin films might be higher than that of Si crystals [24,25]. Yoon et al. measured graphene samples and showed the thermal expansion coefficient of single-layer graphene was estimated with temperature-dependent Raman spectroscopy in the temperature range from 200 to 400 K, the strain caused by the thermal expansion coefficient mismatch between graphene and the substrate played a crucial role in determining the physical properties of graphene [26]. G Ventura and M Perfetti introduced the methods of testing thermal expansion coefficient in details, the new instrument can be used to measure thermal expansion coefficient at low temperature [27]. Herrmann et al. measured thermal expansion of α-HMX, β-HMX, γ-HMX at room temperature, transition temperature respectively and got their linear expansion coefficient [28]. The thermal expansion coefficient of composite materials is also studied, especially the laminar structure materials [29,30]. The thermal expansion coefficient of carbon composites was measured in the temperature range of 303–573 K by thermal diffusivity method [31], and some researchers analyzed the thermal stability [32,33]. Some other materials were used as the substrate, and the curvature method was used to measure the thermal expansion coefficient by molecular perspective [34–37].

In this study, the thermal expansion coefficient of double-base gun propellants with three layers was studied. The theoretical relationships of thermal expansion coefficient between the fast and slow burning layer and the whole composite multi-layered flaky gun propellant in longitudinal were investigated. The thermal expansion coefficient of flaky gun propellant can directly influence the loading density and combustion performance of the gun propellant. Therefore, this study has significance for gun propellant loading, and will increase the understanding of the influence of thermal expansion coefficient on the combustion performance. Testing by TMA in this experiment is different from the method of optical measurement, the variation of specimen thickness is measured directly with precision instrument.

2. Experimental

2.1. Materials

1# double-base absorbent propellant (mass percentage NC (nitrocellulose): 73%, NG (nitroglycerin): 26%, C_2 (Dimethyl diphenylurea): 0.5%, TEGDN (triethylene glycol dinitrate): 0.5%, North Xingan Chem. Co.) and 2# double-base absorbent propellant (NC: 83%, NG: 10%, C_2: 2%, TEGDN: 5%, North Xingan Chem. Co.) were prepared by

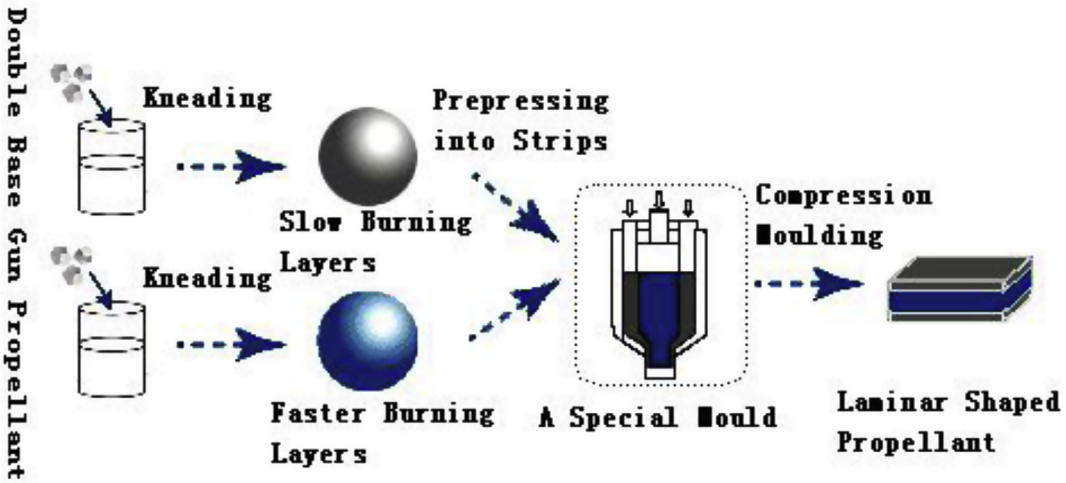

Fig. 1. The preparation of composite multi-layered flaky gun propellant.

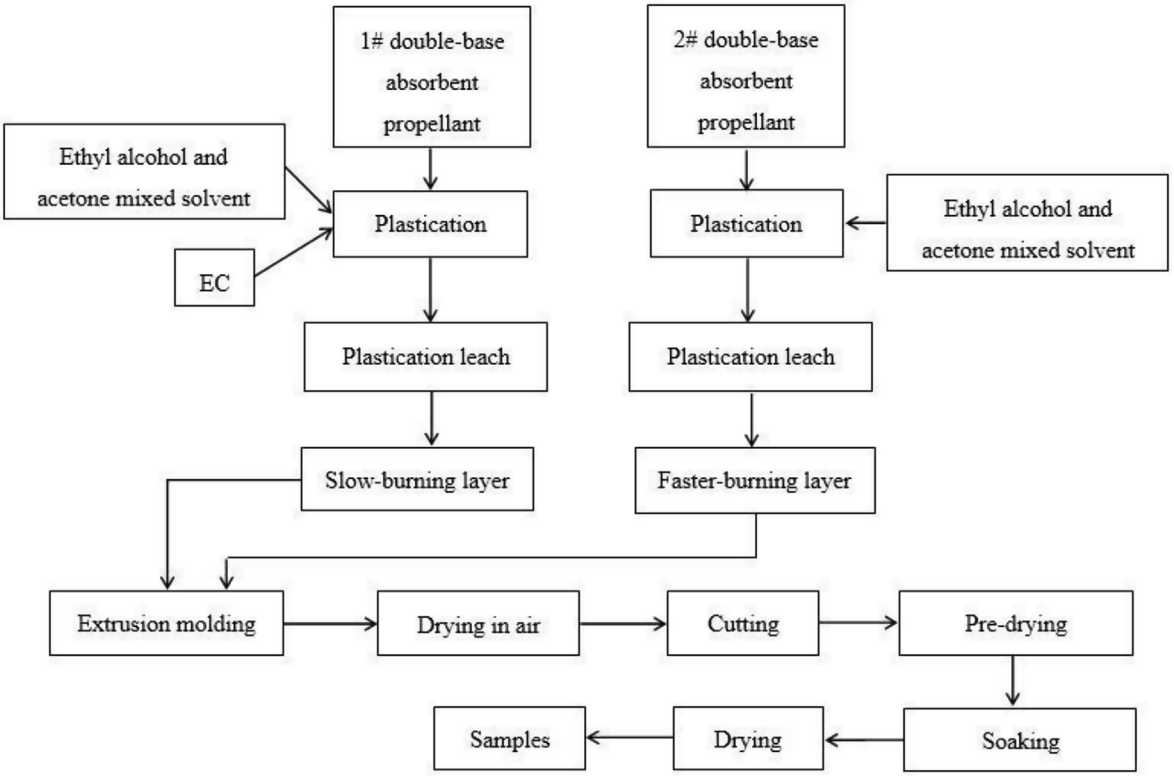

Fig. 2. The flow chart of composite multi-layered flaky gun propellant samples.

methods in Fig. 1, and they were dried at 293 K for 72 h 400 g of 1# and 2# double-base absorbent propellant were weighed and used, respectively. EC (Ethyl cellulose) (North Xingan Chem. Co.) was weighed 35 g and dried for 72 h at 293 K. The mixed solvent (volume fraction 1:0.9, ethyl alcohol and acetone) was 200 mL (see Fig. 2).

2.2. Test samples preparation

The main component of the fast-burning layer material was 1# double-base absorbent propellant. The absorbent propellant and the mixed solvent were stirred in a blade incorporator with cooling water bath for 30–40 min. The slow-burning layer material were composed of high polymer flame retardant (EC) and 2# double-base absorbent propellant, processed in the same method as that of fast-burning layer material. The faster-burning layer and the slow-burning layer materials were preferably blocked in two concentric cylinders mould, respectively, and the composite multi-layered flaky gun propellant was extruded under appropriate pressure (5–8 MPa) through flaky mould. By controlling the flow, the fast-burning layer was three times as thick as the slow-burning layer. The flaky gun propellant was cut into suitable length and dried by blowing hot air at 303 K for 96 h. The preparation diagram is presented in Fig. 1 and the sample description is shown in Table 1.

2.3. TMA measurement

The theory of TMA measurement is based on the deformation of materials that can be obtained as the temperature changes. In some temperature range, the linear thermal expansion coefficient is a constant, TMA can measure the length change (distance between probe and workbench) of materials when the temperature changes, the linear thermal expansion coefficient of material is calculated by measuring the deformation of a material in this temperature range. The schematic diagram of TMA is showed in Fig. 3.

The samples were made by selecting the smooth part from the flaky gun propellant, the samples were flaky shape cuboids with 1 cm in length, 0.5 cm in width, and 0.3–0.6 mm in thickness. The thermal expansion coefficient of the sample was measured by TMA-Q 400 (TA instrument in USA) with a 5 K/min heating rate under dry nitrogen atmosphere over the range of 233–323 K. The thermal expansion coefficient can be expressed by equation (1) [38].

$$\alpha = \frac{\triangle L}{L_0(T_2 - T_1)} = \frac{\triangle L}{L_0 \bullet \triangle T} \tag{1}$$

where α, ΔL, L_0, ΔT are the thermal expansion coefficient, length change, original length, and corresponding temperature change, respectively.

2.4. The theoretical derivation of composite multi-layered flaky gun propellant

Fig. 4 shows the structure of composite multi-layered flaky gun propellant. It is assumed that each layer of the composite multi-layered flaky gun propellant is isotropic (each layer is consisted of a mixture of homogeneous materials). When the temperature rises from T_0 to T, the physical parameters e_0, $2e_1$, $2b_1$ and V change to e_{0_T}, $2e_{1_T}$, $2b_{1_T}$ and V_T, respectively. The change of temperature is ΔT, the thermal expansion coefficient Eq. (1) can be obtained from Eq. (2) [38].

$$\alpha_{e_0} = \frac{e_{0T} - e_0}{e_0 \cdot \Delta T} \quad \alpha_{2e_1} = \frac{2e_{1T} - 2e_0}{2e_1 \cdot \Delta T} \quad \alpha_{b_1} = \frac{2b_{1T} - 2b_1}{2b_1 \cdot \Delta T} \quad \alpha_V = \frac{V_T - V}{V \cdot \Delta T} \tag{2}$$

where e_0 and e_{0_T} are thickness of slow-burning layer, $2e_1$ and $2e_{1_T}$ are thickness of fast-burning layer, $2b_1$ and $2b_{1_T}$ are length changes and width, V and V_T are volume, α_{e_0} is the thermal expansion coefficient of slow-burning layer, α_{e_1} is the thermal expansion coefficient of fast-burning layer.

The volume of the gun propellant at T_0 and T can be determined by Eq. (3) and Eq. (4), respectively:

$$V = (2e_0 + 2e_1) \cdot 2b_1 \cdot 2b_1 = 8(e_0 + e_1)b_1^2 \tag{3}$$

Table 1
The samples label and sample description.

Samples label	Sample description
(1)	0.4 mm thickness of NO.1 composite multi-layered flaky gun propellant
(2)	0.5 mm thickness of NO.1 composite multi-layered flaky gun propellant
(3)	0.6 mm thickness of NO.1 composite multi-layered flaky gun propellant
(4)	0.3 mm thickness of NO.2 composite multi-layered flaky gun propellant
(5)	0.4 mm thickness of NO.2 composite multi-layered flaky gun propellant
(6)	0.5 mm thickness of NO.2 composite multi-layered flaky gun propellant
(7)	0.3 mm thickness slow-burning layer
(8)	0.4 mm thickness slow-burning layer
(9)	0.4 mm thickness fast-burning layer
(10)	0.4 mm of the coated fast-burning layer
(11)	Two layers of 0.4 mm thickness of the laminated fast-burning layer
(12)	Three layers of 0.4 mm thickness of the laminated fast-burning layer
(13)	0.4 mm coated NO.2 composite multi-layered gun propellant
(14)	Two layers of 0.4 mm coating NO.2 composite multi-layered gun propellant
(15)	Three layers of 0.4 mm coating NO.2 composite multi-layered gun propellant

$$V_T = \left[2e_0\left(1+\alpha_{e_0}\Delta T\right)+2e_1\cdot\left(1+\alpha_{e_1}\Delta T\right)\right]\cdot 4b_1^2\left(1+\alpha_{b_1}\Delta T\right)^2 \tag{4}$$

The thermal expansion coefficient is very small, the quadratic of thermal expansion coefficient can be ignored, after simplification, Eq. (4) can be rewritten as Eq. (5):

$$V_T = 8e_0b_1^2\cdot\left(1+2\alpha_{b_1}\Delta T+\alpha_{e_0}\Delta T\right)+8e_1b_1^2\cdot\left(1+2\alpha_{b_1}\Delta T+\alpha_{e_1}\Delta T\right) \tag{5}$$

The volume thermal expansion coefficient can be expressed as Eq. (6),

$$\alpha_V = \frac{2\alpha_{b1}(e_0+e_1)+e_0\alpha_{e0}+e_1\alpha_{e_1}}{e_0+e_1} = 2\alpha_{b1}+\frac{e_0\alpha_{e0}+e_1\alpha_{e_1}}{e_0+e_1}$$
$$= 2\alpha_{b1}+\frac{e_0\alpha_{e0}}{e_0+e_1}+\frac{e_1\alpha_{e1}}{e_0+e_1} \tag{6}$$

As for the volume thermal expansion of composite multi-layered flaky gun propellant, the thermal expansion on z-axis is much bigger than that on x-axis and y-axis, so the thermal expansion on x-axis and y-axis can be ignored, α_{b1} is ignored, Eq. (6) can be rewritten as Eq. (7),

$$\alpha_V = \frac{e_0\alpha_{e0}}{e_0+e_1}+\frac{e_1\alpha_{e1}}{e_0+e_1} \tag{7}$$

And the thermal expansion coefficient in thickness is determined by the proportion of fast-burning layer and slow-burning layer. The proportion of fast-burning layer and slow-burning layer in composite multi-layered flaky gun propellant is defined as δ_f and δ_s, respectively. The relationship between them can be expressed as follows:

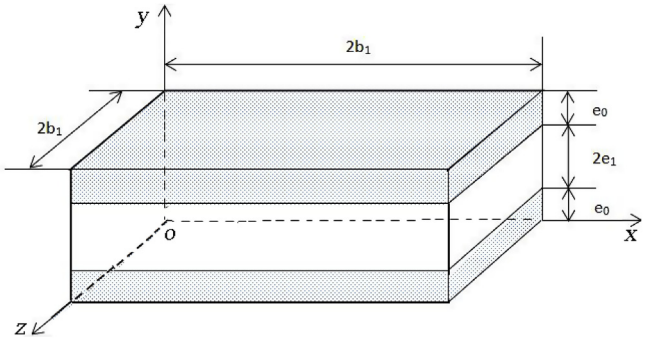

Fig. 4. The shape sketch of composite multi-layered flaky gun propellant.

$$\delta_s+\delta_f = 1 \tag{8}$$

The substitution of Eq. (8) into Eq. (7) results in Eq. (9).

$$\alpha_V = \delta_s\alpha_{e_0}+\delta_f\alpha_{e_1} \tag{9}$$

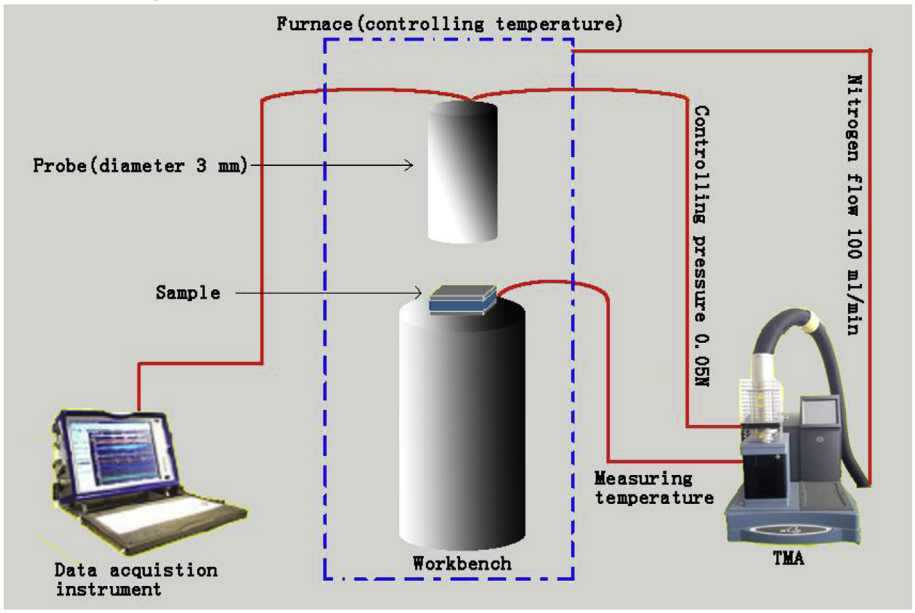

Fig. 3. Schematic diagram of TMA measurement.

According to Eq. (9), it can be inferred that the volume thermal expansion coefficient is determined by linear thermal expansion of fast-burning layer and slow-burning layer, and $\alpha_{e_0} \gg \alpha_{e_1}$ (Experimental result shows that nearly 5–6 times bigger), therefore, in order to decrease the volume thermal expansion coefficient of composite multi-layered flaky gun propellant, the δ_s should be increased and the δ_f should be decreased (Under the premise of ensuring gun propellant performance).

The influence of L_0 is even greater than the influence of materials proportion, L_0 is an order of magnitude bigger than the thermal expansion coefficient, so the influence of L_0 is much bigger than that of thermal expansion. It means that the coated composite multi-layered flaky gun propellant makes the thermal expansion coefficient inapparently decrease. For the laminated composite multi-layered flaky gun propellant, the proportions of fast-burning layer and slow-burning layer were consistent. However, between the two layers of the cellulose, nitrate mixed solvent was added, it means that when the proportion of slow-burning layer (the mixed solvent is main components in slow-burning layer) was increased, δ_s increased a little, and the α_L increased a little, thus the thermal expansion coefficient of laminated composite multi-layered flaky gun propellant unapparent was increased.

3. Results and discussion

3.1. Microscope analysis

In order to determine whether the structure of the composite multi-layered flaky gun propellant matches the theoretical model, a VHX-2000 scanning electron microscope (SEM) (Keyence company in China) was used to observe the sample. Fig. 5 shows the SEM image of composite multi-layered gun propellant. The picture shows that the sample is layered and symmetric. There is a transition layer between fast-burning layer and slow-burning layer. Meanwhile, many grooves are observed on the fast-burning layer, and the faster-burning layer is covered by slow-burning layer tightly. The faster-burning layer and slow-burning layer penetrated each other, thus the surface of fast-burning layer and slow-burning layer was seamless.

The image of SEM shows that the selected sample is smooth, and the sample structure conforms to the theoretical model, this “sandwich type” model is consisted of two slow-burning layer and one fast-burning layer, the fast-burning layer is between tow slow-burning layer as shown in Figss. 4–5 [1,2]. When the material is elongated (or shortened) along the direction of the load, the deformation is shortened (or elongated) in the direction perpendicular to the load, this effect is called Poisson Effect [39]. Because of Poisson Effect, when the composite multi-layered flaky gun propellant is extruded at the outlet of the die, the gun propellant will be extruded in an outlet direction, and the other two directions perpendicular to this direction will be stretched, so the fast-burning layer will be squeezed into the slow-burning layer. In the experiment of this paper, whether the faster-burning and slow-burning layer penetrate each other has an effect on thermal expansion coefficient of whole composite multi-layered flaky propellant is studied.

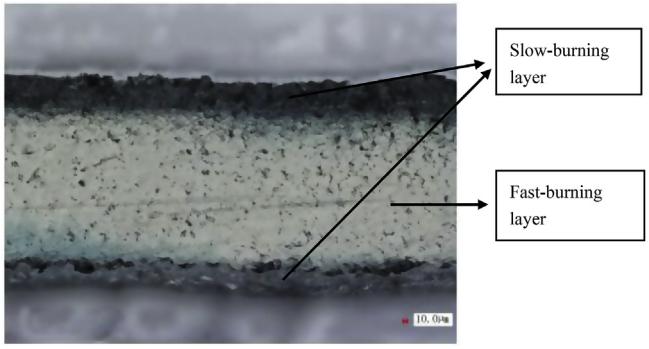

Fig. 5. Microscopic structure of the sample.

Table 2
The value for thermal expansion coefficient of propellant samples (263–283 K).

Samples label (5 samples in each group)	Average thickness L_0/mm	thermal expansion coefficient (the average value) $\alpha/10^{-5}K^{-1}$
(1)	0.4485	6.7331
(2)	0.5356	6.0422
(3)	0.6174	5.4802
(4)	0.3093	3.4460
(5)	0.3997	2.3302
(6)	0.4739	1.8779

where (1), (2), (3) is 0.4 mm, 0.5 mm, 0.6 mm thickness of NO.1 composite multi-layered flaky gun propellant, (4), (5), (6) is 0.3 mm, 0.4 mm, 0.5 mm thickness of NO.2 composite multi-layered gun propellant.

3.2. Thermal expansion coefficient of different sample analysis

The experiment was conducted at 233 K–258 K, the thickness of sample did not have a big change, and the curves had a big vibration. This curve fitting for a straight line may be inaccurate. For example, when the experiment was conducted at 288–303 K, the curves increased slowly, the thickness of sample did not change obviously. When the experiment was conducted at above 303 K, the sample turned soft and shrunk, the curves declined. Because the main ingredients in the composite multi-layered gun propellant was double-based absorption propellant, there was small molecules plasticizer nitroglycerin in the double-based absorption propellant, its glass-transition temperature was relatively low. The probe in the TMA presses the sample with a pressure of 0.05 N, the sample turns to shrink. Therefore, the thermal expansion coefficient is calculated from the data in the temperature range from 263 K to 283 K where the curves are linear, then straight lines are fitted to get L-T curves of various burning-rate gun propellant. The thermal expansion coefficient of sample was calculated using the curves. The data are summarized in Tables 2–5.

3.2.1. The influence of thickness for thermal expansion coefficient

Fig. 6 shows the ΔL-T curves of composite multi-layered flaky gun propellant and Table 2 shows the calculation result of their thermal expansion coefficient. These curves correspond to different thermal expansion curves, and the ratio of the slope to L_0 is the corresponding thermal expansion coefficient, it can be found that the fitting curves have a higher degree of fitting, and the slopes of curves are significantly different. As it is shown in Fig. 6, thermal expansion coefficient of the composite multi-layer gun propellant decreases with the increase of thickness. Due to the main ingredients in the composite multi-layered gun propellant, fast-burning layer holds a large proportion, specifically, three times as much as slow-burning layer. When the thickness increases, the fast-burning layer and slow-burning layer increase at the same time, so the total mass fraction of the fast-burning layer is bigger than that of slow-burning layer, but the thermal expansion coefficient of the fast-burning layer is much smaller than that of the slow-burning layer, so the thermal expansion coefficient of the composite multi-layered flaky gun propellant declines. Thus, it can be seen for the

Table 3
The value for thermal expansion coefficient of propellant samples (263 K–283).

Samples label (5 samples in each group)	Average thickness L_0/mm	thermal expansion coefficient (the average value) $\alpha/10^{-5}K^{-1}$
(7)	0.3147	8.9537
(8)	0.4521	6.3739
(9)	0.4469	1.6531

where (7) (8) is 0.3 mm, 0.4 mm thickness slow-burning layer, (9) is 0.4 mm thickness fast-burning layer.

Table 4
The value for thermal expansion coefficient of propellant samples (263–283 K).

Samples label (5 samples in each group)	Average thickness L_0/mm	thermal expansion coefficient (the average value) $\alpha/10^{-5}K^{-1}$
(9)	0.4469	1.6531
(10)	0.5245	7.6542
(11)	1.1414	18.8341
(12)	1.4162	18.7408

where (9) is 0.4 mm thickness of the fast-burning layer, (10) is 0.4 mm of the coated fast-burning layer, (11), (12) is two layers and three layers of 0.4 mm thickness of the laminated fast-burning layer.

Table 5
The value for thermal expansion coefficient of propellant samples (263–283 K).

Samples label (5 samples in each group)	Average thickness L_0/mm	thermal expansion coefficient (the average value) $\alpha/10^{-5}K^{-1}$
(5)	0.4521	6.3739
(13)	0.6224	1.6832
(14)	1.0968	2.3412
(15)	1.4060	2.7552

composite multi-layer gun propellant of the same material, when its thickness increases, its thermal expansion coefficient declines.

3.2.2. The thermal expansion coefficient of fast-burning layer and slow-burning layer

Fig. 7 shows the curves of fast and slow burning layer. The calculation results of their thermal expansion coefficient are summarized in Table 3 From Fig. 7, we can conclude that the thermal expansion coefficient of the slow-burning layer is much greater than that of the fast-burning layer. Due to some difference in the ingredient of slow-burning layer, on the basis of fast-burning layer, it contains 10% flame retardant (EC), thus in the process of temperature rising, the coiled molecular chain will be extended because of the Elastic Effect, which makes the thermal expansion coefficient of the slow-burning layer much greater than that of the fast-burning layer (see Fig. 8).

3.2.3. The influence of coating and laminating on the thermal expansion coefficient of fast-burning layer

In order to ensure the uniformity of the samples, the laminated samples were used to test the change of thermal expansion coefficient. The preparation of laminated samples required applying solvent between the layers, so the effects of coating samples on the thermal expansion coefficient were needed to test.

Fig. 9 shows the curves of coated fast-burning layer samples and Table 4 shows the calculation result of their thermal expansion

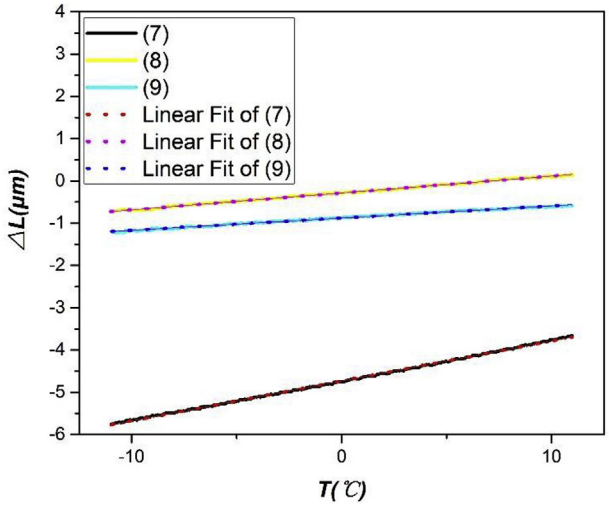

Fig. 7. ΔL-T curves for fast and slow burning layer.

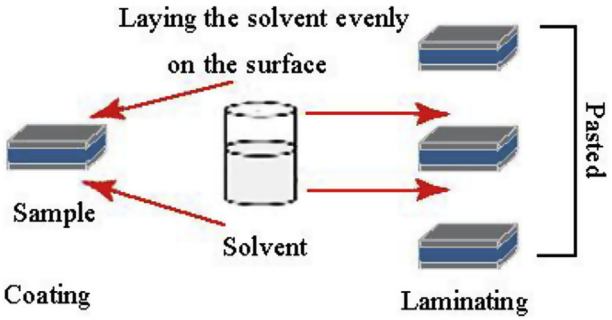

Fig. 8. Schematic diagram of the coated and laminated samples.

coefficient. From Fig. 6, which corresponds to (9), (10), (11), (12), we can conclude that the thermal expansion coefficient of the coated fast-burning layer increases. Since the coating was made by using a layer of solvent (dissolve the nitrocellulose with acetone solution) on both side of the fast-burning layer, the nitrocellulose was the main ingredients of solvent and the same was for the slow-burning layer. It will be equal to add the slow-burning layer to the fast-burning layer, and the thermal expansion coefficient of the slow-burning layer is greater than that of the fast-burning layer, so its thermal expansion coefficient increases. When the number of layers of laminated fast-burning layer increases, the numbers of layers of same material has no effect on the thermal expansion coefficient, the thermal expansion coefficient does not change obviously, thus it can be seen that the number of layers of

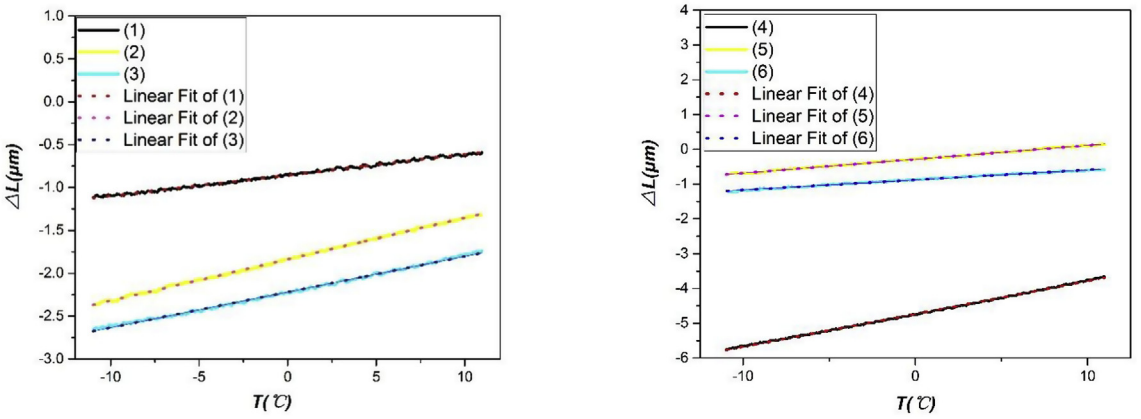

Fig. 6. ΔL-T curves for composite multi-layered flaky gun propellant.

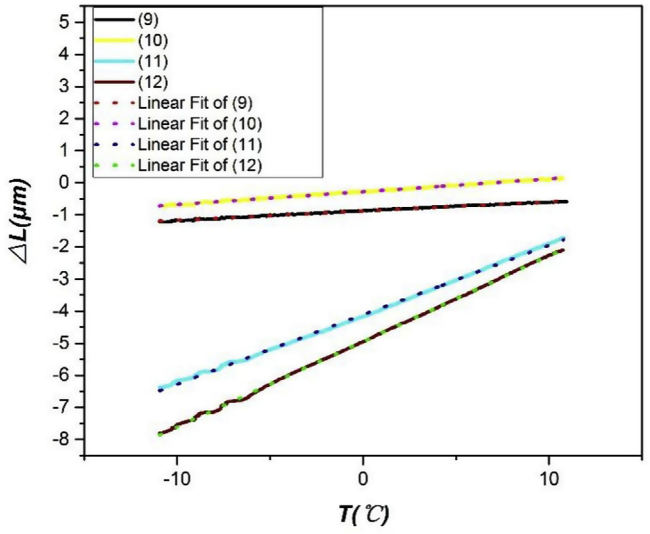

Fig. 9. ΔL-T curves for coated and laminated fast-burning layer samples.

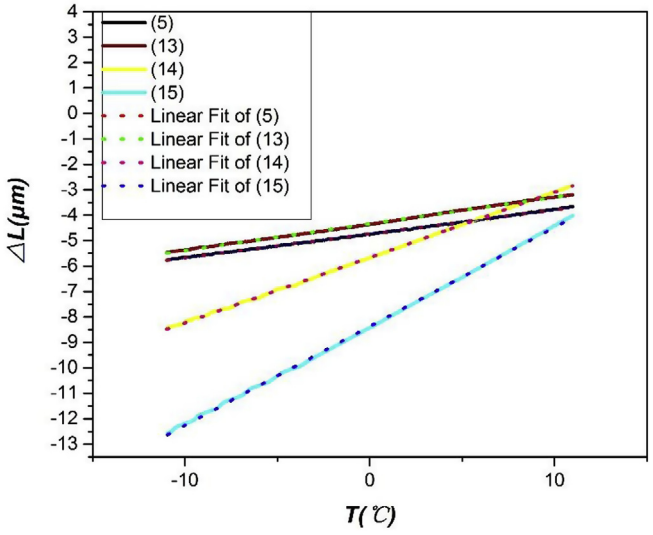

Fig. 10. ΔL-T curves for coated and laminated gun propellant samples.

lamination has a small influence on the thermal expansion coefficient of fast-burning layer.

3.2.4. The influence of coating and laminating for thermal expansion coefficient of composite multi-layered gun propellant

Fig. 10 shows the curves of the laminated propellant samples and Table 5 shows the calculated results of their thermal expansion coefficient. From Fig. 7 which corresponds to (5), (13), (14), (15), we can conclude that after coating, the thermal expansion coefficient of the composite multi-layered flaky gun propellant declines, and after laminating, the thermal expansion coefficient of composite multi-layered flaky gun propellant basically stays the same. The reason is that for the coated composite multi-layered flaky gun propellant, its thickness increases, the proportion of fast-burning layer and its thickness increases, so its thermal expansion coefficient declines. As for the laminating composite multi-layered flaky gun propellant, the thickness of slow-burning layer increases, but fast-burning layer is the major proportion, so its thermal expansion coefficient does not change obviously.

Compared with the test result by Zhang, the thermal expansion coefficients of composite multi-layered flaky gun propellants and double-layered variable burning-rate gun propellant have the same order of magnitude ($1 \times 10^{-5} K^{-1}$), meanwhile, the result showed that the thermal expansion coefficient of slow-burning layer is higher than that of fast-burning layer [40].where (5) is 0.4 mm thickness of the NO.2 composite multi-layered gun propellant, (13) is 0.4 mm coated NO.2 composite multi-layered gun propellant, (14), (15) is two layers and three layers of 0.4 mm coating NO.2 composite multi-layered gun propellant.

4. Conclusion

The average thermal expansion coefficient of this kind composite multi-layered flaky gun propellant is $1 \times 10^{-5} K^{-1}$ from 263 to 283 K, at the thickness of 0.4 mm. For 0.4 mm gun propellant, coating makes the thermal expansion coefficient reduced, the laminating makes the thermal expansion coefficient reduce inapparently. For the fast-burning layer, coating makes the thermal expansion coefficient increase, the laminating makes the thermal expansion coefficient increase, but there is no obvious relationship with numbers of layers. In this study, the calculation model is based on the structure of the gun propellant type. Theoretically, this calculation model can be applied to determinate the thermal expansion coefficient of materials with similar structure, these materials can include the ceramic, carbon, metals [41–53], polymers [53–56] and their colloids and nanocoposites [57–78].

References

[1] Xiao Z, He Z, Liu Y, Ma Z, Lü B. Principle and realizable approach of variable burning rate propellant. Chin J Explos Propellants 2005;28:25–7.
[2] He Z, Liu Y, Ma Z, Lu B, Xiao Z. Combustion property character of variable-burning rate gun propellant. Chin J Explos Propellants 2004;27:10–2.
[3] Zhang Z. Measurement of thermal expansion coefficients with holographic technique. J Therm Sci 1995;4(1):67–74.
[4] Okaji M, Yamada N, Kato H, Nara K. Measurements of linear thermal expansion coefficients of copper srm 736 and some commercially available coppers in the temperature range 20-300 k by means of an absolute interferometric dilatometer. Bull NRLM 1997;46(5):251–4.
[5] Strycker M, Schueremans L, Paepegem W, Debruyne D. Measuring the thermal expansion coefficient of tubular steel specimens with digital image correlation techniques. Optic Laser Eng 2010;48(10):978–86.
[6] Forrest J, Dalnoki-Veress K, Stevens J, et al. Effect of free surfaces on the glass transition temperature of thin polymer films. Phys Rev Lett 1996;77(10):2002–5.
[7] Huang H, Xu Y, Hong Y. Effects of film thickness on moisture sorption, glass transition temperature and morphology of poly (chloro-p-xylylene) film. Polymer 2005;46(16):5949–55.
[8] Segal L. The thermal expansion of reinforced nylon-6 composites through the matrix glass transition temperature. Polym Eng Sci 1979;19(5):365–72.
[9] Hasegawa M, Koyanaka M. Polyimides containing trans1,4-cyclohexane unit. polymerizability of their precursors and low-CTE, low-K and high-Tg properties. High Perform Polym 2003;15(1):47–64.
[10] Sleight A. Negative thermal expansion material. Curr Opin Solid State Mater Sci 1998;3(2):128–31.
[11] Lind C. Two decades of negative thermal expansion research: where do we stand? Materials 2012;5(6):1125–54.
[12] Roy R, Agrawal D, Mckinstry H. Very low thermal expansion coefficient materials. Annu Rev Mater Res 1989;19:59–81.
[13] Marinkovic B, Ari M, Avillez R, et al. Correlation between AO6 polyhedral distortion and negative thermal expansion in orthorhombic $Y_2Mo_3O_{12}$ and related materials. Chem Mater 2009;21:2886–94.
[14] Wang L, Wang F, Yuan P, et al. Negative thermal expansion correlated with polyhedral movements and distortions in orthorhombic $Y_2Mo_3O_{12}$. Mater Res Bull 2013;48(7):2724–9.
[15] Amos T, Yokochi A, Sleight A. Phase transition and negative thermal expansion in tetragonal $NbOPO_4$. J Solid State Chem 1998;141(1):303–7.
[16] Jie S, Shu X, Yu L, et al. Investigation on the thermal expansion and theoretical density of 1,3,5-Trinitro-1,3,5-Triazacyclohexane. Propellants, Explos Pyrotech 2011;36(4):341–6.
[17] Lu N, Oza S. A comparative study of the mechanical properties of hemp fiber with virgin and recycled high density polyethylene matrix. Compos B Eng 2013;45(1):1651–6.
[18] Lu N, Oza S. Thermal stability and thermo-mechanical properties of hemp-high density polyethylene composites: effect of two different chemical modifications. Compos B Eng 2013;44(1):484–90.
[19] Zakharchenko K, Katsnelson M, Fasolino A. Finite temperature lattice properties of graphene beyond the quasiharmonic approximation. Phys Rev Lett 2009;102(4):046808.
[20] Lim T. Negative thermal expansion structures constructed from positive thermal expansion trusses. J Mater Sci 2012;47(1):368–73.
[21] Grima J, Ellul B, Attard D, et al. Composites with needle-like inclusions exhibiting negative thermal expansion: a preliminary investigation. Compos Sci Technol

2010;70(16):2248–52.
[22] Bhattacharya S, Saha B. Uniaxial negative thermal expansion in an organic complex caused by sliding of layers. Cryst Growth Des 2012;12(10):1187–91.
[23] Nicolaï B, Rietveld I, Barrio M, et al. Uniaxial negative thermal expansion in crystals of tienoxolol. Struct Chem 2013;24(1):279–83.
[24] Tada H, Kumpel A, Lathrop R, et al. Thermal expansion coefficient of polycrystalline silicon and silicon dioxide thin films at high temperatures. J Appl Phys 2000;87(9):4189–93.
[25] Feng Y, Jiang X, Ghafari E, et al. Metal oxides for thermoelectric power generation and beyond. Adv Compos Hybrid Mater 2018;1(1):114–26.
[26] Yoon D, Son Y, Cheong H. Negative thermal expansion coefficient of graphene measured by Raman spectroscopy. Nano Lett 2011;11(8):3227–31.
[27] Ventura G, Perfetti M. How to measure the thermal expansion coefficient at low temperatures, thermal properties of solids at room and cryogenic temperatures. Springer Netherlands; 2014. p. 93–120.
[28] Herrmann M, Engel W, Eisenreich N. Thermal expansion, transitions, sensitivities and burning rates of hmx. Propellants, Explos Pyrotech 2010;17(4):190–5.
[29] Giddings P, Bowen C, Salo A, Kim H, Ive A. Bistable composite laminates: effects of laminate composition on cured shape and response to thermal load. Compos Struct 2010;92(9):2220–5.
[30] Moore Z, Siaei-Rad A, Salehi H. Thermal response and stability characteristics of bistable composite;laminates by considering temperature dependent material properties and resin layers. Appl Compos Mater 2013;20(1):87–106.
[31] Chukov D, Stepashkin A, Salimon A, Kaloshkin S. Highly filled elastomeric matrix composites: structure and property evolution at low temperature carbonization. Mater Des 2018;156:22–31.
[32] Oza S, Ning H, Ferguson I, et al. Effect of surface treatment on thermal stability of the hemp-PLA composites: correlation of activation energy with thermal degradation. Compos B Eng 2014;67:227–32.
[33] Lu N, Ferguson I. III-nitrides for energy production: photovoltaic and thermoelectric applications. Semicond Sci Technol 2013;28(7):074023.
[34] Besozzi E, Dellasega D, Pezzoli A, et al. Coefficient of thermal expansion of nanostructured tungsten based coatings assessed by substrate curvature method. Mater Des 2017;137:192–203.
[35] Liu J, Gong Y, Wang J, et al. Realization of zero thermal expansion in La(Fe, Si)$_{13}$-based system with high mechanical stability. Mater Des 2018;148:71–7.
[36] Shi J, Cai K, Xie Y. Thermal and tensile properties of diamondene at finite temperature: a molecular dynamics study. Mater Des 2018;156:125–34.
[37] Zhao H, Chen L, Yun J, Tang L, Wen Z, Zhang X, Gu J. Improved thermal stabilities, ablation and mechanical properties for carbon fibers/phenolic resins laminated composites modified by silicon-containing polyborazine. Eng Sci 2018;2:57–66. crossref: www.doi.org/10.30919/es8d726.
[38] Miao E, Fei Y. Reasoning of limitation about tradition coefficient of thermal expansion. J Heilongjiang Institute Sci Technol 2003;13(1):1–3.
[39] Moulin D, Roche RL. Correction of the Poisson effect in the elastic analysis of low-cycle fatigue. Int J Press Vessel Pip 1985;19(3):213–33.
[40] Zhang L, Wang P, He L, Hang L. Experimental study on relationship of linear expansion coefficient for variable burning-rate gun propellant. Chin J Explos Propellants 2011;34(2):80–3.
[41] Zhao Z, Bai P, Li L, Li J, Wu L, Huo P, Tan L. The reaction thermodynamics during plating Al on graphene process. Materials 2019;12(2):330.
[42] Zhao Z, Guan R, Zhang J, Zhao Z, Bai P. Effects of process parameters of semisolid stirring on microstructure of Mg-3Sn-1Mn-3SiC (wt%) strip processed by rheo-rolling. Acta Metall Sin 2017;30:66–72.
[43] Zhao Z, Bai1 P, Guan R, et al. Microstructural evolution and mechanical strengthening mechanism of Mg-3Sn-1Mn-1La alloy after heat treatments. Mater Sci Eng, A 2018;734:200–9.
[44] Zhao Y, Qi L, Jin Y, Wang K, Tian J, Han P. The structural, elastic, electronic properties and Debye temperature of D0$_{22}$-Ni$_3$V under pressure from first-principles. J Alloy Comp 2015;647:1104–10.
[45] Zhao Y, Zhang B, Hou H, Chen W, Wang M. Phase-field simulation for the evolution of solid/liquid interface front in directional solidification process. J Mater Sci Technol 2019. https://doi.org/10.1016/j.jmst.2018.12.009.
[46] Zhao Y, Deng S, Liu H, et al. First-principle investigation of pressure and temperature influence on structural, mechanical and thermodynamic properties of Ti_3AC_2 (A = Al and Si). Comput Mater Sci 2018;154:365–70.
[47] Zhao Y, Tian X, Zhao B, et al. Precipitation sequence of middle Al concentration alloy using the inversion algorithm and microscopic phase field model. Sci Adv Mater 2018;10:1793–804.
[48] Kirubasankar B, Murugadoss V, Lin J, et al. In-situ grown nickel selenide onto graphene nanohybrid electrodes for high energy density asymmetric supercapacitors. Nanoscale 2018;10:20414–25.
[49] Zhao W, Li X, Yin R, et al. Urchin-like NiO-$NiCo_2O_4$ heterostructure microsphere catalysts for enhanced rechargeable non-aqueous Li-O_2 batteries. Nanoscale 2019;11:50–9.
[50] Du W, Wang X, Zhan J, et al. Biological cell template synthesis of nitrogen-doped porous hollow carbon spheres/MnO_2 composites for high-performance asymmetric supercapacitors. Electrochim Acta 2019;296:907–15.
[51] Idrees M, Batool S, Kong J, et al. Polyborosilazane derived ceramics - nitrogen sulfur dual doped graphene nanocomposite anode for enhanced lithium ion batteries. Electrochim Acta 2019;296:925–37.
[52] Qu Z, Shi M, Wu H, et al. An efficient binder-free electrode with multiple carbonized channels wrapped by NiCo2O4 nanosheets for high-performance capacitive energy storage. J Power Sources 2019;410–411:179–87.
[53] Sheng Y, Yang J, Wang F, et al. Sol-gel synthesized hexagonal boron nitride/titania nanocomposites with enhanced photocatalytic activity. Appl Surf Sci 2019;465:154–63.
[54] Wang C, Mo B, He Z, et al. Hydroxide ions transportation in polynorbornene anion exchange membrane. Polymer 2018;138:363–8.
[55] Wang C, He Z, Xie X, et al. Controllable cross-linking anion exchange membranes with excellent mechanical and thermal properties. Macromol Mater Eng 2018;3:1700462.
[56] Wang C, Mo B, He Z, et al. Crosslinked norbornene copolymer anion exchange membrane for fuel cells. J Membr Sci 2018;556:118–25.
[57] Wang L, Qiu H, Liang C, et al. Electromagnetic interference shielding MWCNT-Fe_3O_4@Ag/epoxy nanocomposites with satisfactory thermal conductivity and high thermal stability. Carbon 2019;141:506–14.
[58] Gu H, Zhang H, Ma C, et al. Trace electrosprayed nanopolystyrene facilitated dispersion of multiwalled carbon nanotubes: simultaneously strengthening and toughening epoxy. Carbon 2019;142:131–40.
[59] Du H, Zhao C, Lin J, et al. Carbon nanomaterials in direct liquid fuel cells. Chem Rec 2018;18:1365–72.
[60] Li Y, Jing T, Xu G, et al. 3-D magnetic graphene oxide-magnetite poly(vinyl alcohol) nanocomposite substrates for immobilizing enzyme. Polymer 2018;149:13–22.
[61] Zhao J, Wu L, Zhan C, Shao Q, Guo Z, Zhang L. Overview of polymer nanocomposites: computer simulation understanding of physical properties. Polymer 2017;133:272–87.
[62] Li Z, Wang B, Qin X, et al. Superhydrophobic/superoleophilic polycarbonate/carbon nanotubes porous monolith for selective oil adsorption from water. ACS Sustainable Chem Eng 2018;6:13747–55.
[63] Qian Y, Yuan Y, Wang H, et al. Highly efficient uranium adsorption by salicylaldoxime/polydopamine graphene oxide nanocomposites. J Mater Chem 2018;6:24676–85.
[64] Liu H, Li Q, Zhang S, et al. Electrically conductive polymer composites for smart flexible strain sensor: a critical review. J Mater Chem C 2018;6:12121–41.
[65] Wei H, Wang H, Xia Y, et al. An overview of lead-free piezoelectric materials and devices. J Mater Chem C 2018;6:12446–67.
[66] He Y, Yang S, Liu H, et al. Reinforced carbon fiber laminates with oriented carbon nanotube epoxy nanocomposites: magnetic field assisted alignment and cryogenic temperature mechanical properties. J Colloid Interf Sci 2018;517:40–51.
[67] Wang C, Murugadoss V, Kong J, et al. Overview of carbon nanostructures and nanocomposites for electromagnetic wave shielding. Carbon 2018;140:696–733.
[68] Jiang D, Murugadoss V, Wang Y, et al. Electromagnetic interference shielding polymers and nanocomposites – a review. Polym Rev 2019. https://doi.org/10.1080/15583724.2018.1546737. in press.
[69] Wu Z, Gao S, Chen L, et al. Electrically insulated epoxy nanocomposites reinforced with synergistic core-shell SiO_2@MWCNTs and montmorillonite bifillers. Macromol Chem Phys 2017;218:1700357.
[70] Wu Z, Cui H, Chen L, et al. Interfacially reinforced unsaturated polyester carbon fiber composites with a vinyl ester-carbon nanotubes sizing agent. Compos Sci Technol 2018;164:195–203.
[71] Wu N, Liu C, Xu D, et al. Ultrathin high-performance electromagnetic wave absorbers with facilely fabricated hierarchical porous Co/C crabapples. J Mater Chem C 2019;7:1659–69. https://doi.org/10.1039/C8TC04984J. in press.
[72] Xie W, Zhu X, Yi S, Kuang J, Cheng H, Tang W, Deng Y. Electromagnetic absorption properties of natural microcrystalline graphite. Mater Des 2016;90(1):38–46.
[73] Zhang J, Li P, Zhang Z, et al. Solvent-free graphene liquids: promising candidates for lubricants without the base oil. J Colloid Interf Sci 2019;542:159–67.
[74] Jiao Y, Zhang J, Liu S, Liang Y, Li S, Zhou H, Zhang J. The graphene oxide ionic solvent-free nanofluids and their battery performances. Sci Adv Mater 2018;10:1706–13.
[75] Liu M, Li B, Zhou H, Chen C, Liu Y, Liu T. Extraordinary rate capability achieved by a 3D "skeleton/skin" carbon aerogel-polyaniline hybrid with vertically aligned pores. Chem Comm 2017;53:2810–3.
[76] Li J, Ge S, Wang J, et al. Water-based rust converter and its polymer composites for surface anticorrosion. Colloids Surf A: Physicochem Eng Aspects 2018;537:334–42.
[77] Guo X, Ge S, Wang J, et al. Waterborne acrylic resin modified with glycidyl methacrylate (GMA): formula optimization and property analysis. Polymer 2018;143:155–63.
[78] Dong M, Li Q, Liu H, et al. Thermoplastic polyurethane-carbon black nanocomposite coating: fabrication and solid particle erosion resistance. Polymer 2018;158:381–90.